

# Exact boundary-value solution for an electromagnetic wave propagating in a linearly-varying index of refraction

N. A. Lopez<sup>1</sup>

<sup>1</sup>Rudolf Peierls Centre for Theoretical Physics, University of Oxford, Oxford OX1 3PU, UK

(Received xx; revised xx; accepted xx)

The propagation of electromagnetic waves in a linearly-varying index of refraction is a fundamental problem in wave physics, being relevant in fusion science for describing certain wave-based heating and diagnostic schemes. Here, an exact solution is obtained for a given incoming wavefield specified on the boundary transverse to the direction of inhomogeneity by performing a spectral, rather than asymptotic, matching. Two case studies are then presented: a Gaussian beam at oblique incidence and a speckled wavefield at normal incidence. For the Gaussian beam, it is shown that when the waist  $W$  is sufficiently large, oblique incidence manifests simply as rigid translation and focal shift of the corresponding diffraction pattern at normal incidence. The destruction of the hyperbolic umbilic caustic (corresponding to a critically focused beam) as  $W$  is reduced is then demonstrated. The caustic disappears once  $W \lesssim \delta_a \sqrt{L}$  ( $L$  being the medium lengthscale normalized by the Airy skin depth  $\delta_a$ ), at which point the wave behavior is increasingly described by Airy functions, but experiences less focusing as a result. To maximize the intensity of a launched Gaussian beam at a turning point, one should therefore minimize the imaginary part of the launched complex beam parameter while having the real part satisfy critical focusing. For the speckled wavefield, it is shown that the transverse speckle pattern only couples to the Airy longitudinal pattern when the coupling parameter  $\eta = \sqrt{L}/f_{\#}$  is large, with  $f_{\#}$  being the f-number of the launching aperture. When  $\eta \ll 1$ , a reduced description of the total wavefield can be obtained by simply multiplying the incoming speckle pattern with the Airy swelling.

## 1. Introduction

The description of an electromagnetic wave propagating in a linearly-varying medium is a classic problem in wave physics, sometimes referred to as the linear-layer problem (Ginzburg 1961). Its relevance to plasma physics and fusion research is predominantly as a local description near a turning point for wave-based heating and diagnostics applications. For example, a recently developed scheme to perform fundamental X-mode heating and current drive in startup plasmas (Ono *et al.* 2022a,b) involves an obliquely launched X-mode resonating with electrons near the low-density cutoff; the efficiency of the heating process will therefore depend on the wavefield intensity behavior near the cutoff. Similarly, the Doppler backscattering diagnostic (Hall-Chen *et al.* 2022) relies on the swelling of a wavefield near a turning point to probe turbulence spectra via nonlinear scattering of the diagnostic beam; the intensity details near the turning point therefore determine the diagnostic sensitivity and localization.

Many authors (Ginzburg 1961; Orlov and Tropkin 1980; Maj *et al.* 2009, 2010; Lopez *et al.* 2023) have obtained solutions to the linear-layer problem in terms of a prescribed field  $\psi$  along the boundary  $z = 0$ , where  $z$  is the direction of medium inhomogeneity.

However, the full field  $\psi$  is made up of both the incoming and reflected components, and often only the incoming component is known in practice. To remedy this apparent shortcoming in the obtained solutions, most of the aforementioned authors performed an asymptotic matching to isolate only the incoming component. This resolves the issue with the boundary condition, but at the cost of introducing an asymptotic validity criterion into the analysis: the resulting formulas are not valid when the incoming field is specified too close to the turning point, as might occur when beams are launched obliquely. A universally valid formula that matches to a prescribed incoming field would be more desirable for use in applications.

Here we obtain such a formula by performing the matching spectrally instead of asymptotically. No new asymptotic validity criteria are introduced into the problem, and it is shown explicitly that the obtained solution exactly reproduces the incoming wavefield at the boundary, regardless the distance between the boundary and the turning point. The solution involves an integral whose kernel contains the standard Airy function, which is expected to arise in this problem, and also the related Scorer function, which is less well-known. To demonstrate the flexibility of the new solution, two special cases are considered: an obliquely launched Gaussian beam and a normally incident speckled wavefield produced by a bilevel random phase plate (RPP). For this first example, it is shown how the hyperbolic umbilic caustic created at critical focusing gets degraded as the beam waist becomes smaller for a variety of injection angles, including angles at which the asymptotic validity criterion for the previous solutions is violated. For the second example, an explicit coupling parameter is derived and demonstrated that governs whether the speckles influence the behavior of the wavefield near the turning point. Both these examples can serve as starting points to developing reduced models of waves near turning points with more comprehensive physics content, which would be useful for the fusion applications mentioned in the first paragraph, among other applications.

This paper is organized as follows. In Sec. 2 the linear-layer problem is introduced. In Sec. 3 a spectral matching is performed to allow the solution to the linear-layer problem to be expressed only in terms of the incoming field at the boundary. This is the main result of this paper. In Sec. 4 the special case of an incoming Gaussian beam is studied, with particular emphasis on its behavior near critical focusing. In Sec. 5 the special case of an incoming speckled wavefield is studied, with focus on characterizing the coupling between speckles and the Airy pattern. Finally, Sec. 6 summarizes the main conclusions. Auxiliary calculations are presented in appendices.

## 2. Background

Let us consider an electromagnetic wave propagating in  $N + 1$  spatial dimensions in a medium whose index of refraction varies as a linear function. We take one dimension, denoted  $z$ , to be aligned with the direction of inhomogeneity, and label the remaining  $N$  dimensions by the vector  $\mathbf{x}$ . Assuming time-harmonic modes with a single angular frequency  $\omega$ , the wavefield amplitude can be shown to satisfy the Helmholtz equation

$$\partial_{\mathbf{x}}^2 \psi(\mathbf{x}, z) + \partial_z^2 \psi(\mathbf{x}, z) + \frac{\ell - z}{\delta_a^3} \psi(\mathbf{x}, z) = 0, \quad (2.1)$$

where  $\delta_a$  is a constant with units of length sometimes called the ‘Airy skin depth’ (Michel 2023). In terms of the angular frequency  $\omega$ , the medium lengthscale  $\ell$ , and the speed of light in vacuum  $c$ ,  $\delta_a$  is given as

$$\delta_a = \sqrt[3]{\frac{\ell c^2}{\omega^2}}. \quad (2.2)$$

We shall maintain  $N$  unspecified in the following analysis, but note that practical calculations will have either  $N = 1$  or  $N = 2$  for 2-D or 3-D propagation, respectively. We shall also only seek solutions that are stable, such that they become evanescent and decay to zero as  $z \rightarrow +\infty$  (i.e., we shall impose a radiation boundary condition).

Let us now introduce normalized spatial coordinates

$$\mathbf{x} = \delta_a \mathbf{X}, \quad z = \delta_a Z, \quad \ell = \delta_a L, \quad (2.3)$$

such that Eq. (2.1) becomes

$$\partial_{\mathbf{X}}^2 \psi(\mathbf{X}, Z) + \partial_Z^2 \psi(\mathbf{X}, Z) + (L - Z)\psi(\mathbf{X}, Z) = 0. \quad (2.4)$$

Let us also adopt the following convention for the Fourier transform (FT):

$$\tilde{\psi}(\mathbf{K}_x, K_z) = \int \frac{d\mathbf{X} dZ}{(2\pi)^{N+1}} \psi(\mathbf{X}, Z) e^{-i\mathbf{K}_x \cdot \mathbf{X} - iK_z Z}, \quad (2.5a)$$

$$\psi(\mathbf{X}, Z) = \int d\mathbf{K}_x dK_z \tilde{\psi}(\mathbf{K}_x, K_z) e^{i\mathbf{K}_x \cdot \mathbf{X} + iK_z Z}. \quad (2.5b)$$

Taking the FT of Eq. (2.4) then gives

$$i\partial_{K_z} \tilde{\psi}(\mathbf{K}_x, K_z) = (L - |\mathbf{K}_x|^2 - K_z^2) \tilde{\psi}(\mathbf{K}_x, K_z), \quad (2.6)$$

with solution given by

$$\tilde{\psi}(\mathbf{K}_x, K_z) = \tilde{\psi}_0(\mathbf{K}_x) \exp \left[ i \frac{K_z^3}{3} + i (|\mathbf{K}_x|^2 - L) K_z \right]. \quad (2.7)$$

Here,  $\tilde{\psi}_0(\mathbf{K}_x) \equiv \tilde{\psi}(0, \mathbf{K}_x)$  is an arbitrary function that can eventually be matched to boundary conditions, as we show in the next section.

The general solution to Eq. (2.4) is then obtained by taking an inverse FT of Eq. (2.7):

$$\psi(\mathbf{X}, Z) = \int d\mathbf{K}_x dK_z \tilde{\psi}_0(\mathbf{K}_x) \exp \left[ i \frac{K_z^3}{3} + i (|\mathbf{K}_x|^2 + Z - L) K_z + i\mathbf{K}_x \cdot \mathbf{X} \right]. \quad (2.8)$$

Note that the radiation boundary condition has been tacitly imposed through our use of an FT to obtain the solution (2.8).

### 3. Boundary-value solution for prescribed incoming wavefield

#### 3.1. Isolating the incoming contribution

Although Eq. (2.8) constitutes the general boundary-value solution for a prescribed  $\tilde{\psi}_0(\mathbf{K}_x)$ , this boundary-value solution is formulated in the spectral domain, which is not useful for most applications. Here we shall instead obtain the boundary-value solution in the coordinate domain by prescribing an incoming wavefield, since this is often what is known in practice.

To do this, consider the field on the  $Z = 0$  plane, i.e.,  $\psi(\mathbf{X}, 0)$ . We can split this into ‘incoming’ and ‘outgoing’ components by using a spectral filter based on the sign of  $K_z$  as follows:

$$\psi_{\text{in}}(\mathbf{X}) = \int d\mathbf{K}_x \tilde{\psi}_0(\mathbf{K}_x) e^{i\mathbf{K}_x \cdot \mathbf{X}} \int_0^\infty dK_z \exp \left[ i \frac{K_z^3}{3} + i (|\mathbf{K}_x|^2 - L) K_z \right], \quad (3.1a)$$

$$\psi_{\text{out}}(\mathbf{X}) = \int d\mathbf{K}_x \tilde{\psi}_0(\mathbf{K}_x) e^{i\mathbf{K}_x \cdot \mathbf{X}} \int_{-\infty}^0 dK_z \exp \left[ i \frac{K_z^3}{3} + i (|\mathbf{K}_x|^2 - L) K_z \right]. \quad (3.1b)$$

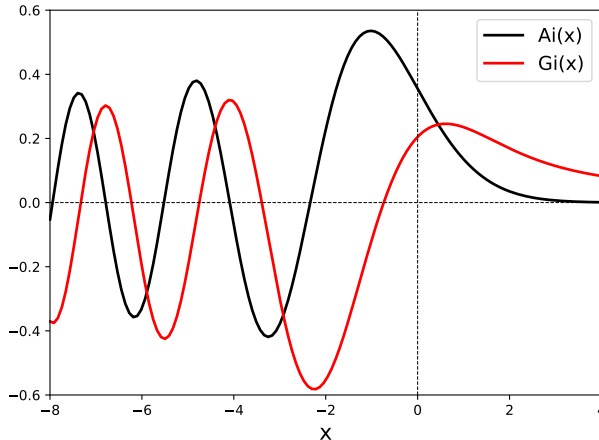


**Figure 1:** The Airy function  $\text{Ai}(x)$  and the Scorer function  $\text{Gi}(x)$  plotted against their argument. Both functions behave qualitatively similar, exhibiting exponential decay for  $x > 0$  and oscillatory behavior (with relative phase shift) for  $x < 0$ .

One then has the exact decomposition

$$\psi(\mathbf{X}, 0) = \psi_{\text{in}}(\mathbf{X}) + \psi_{\text{out}}(\mathbf{X}). \quad (3.2)$$

To proceed further, one is required to compute the integral

$$\begin{aligned} I(\zeta) &= \int_0^\infty dK_z \exp\left(i\frac{K_z^3}{3} + i\zeta K_z\right) \\ &\equiv \int_0^\infty dK_z \cos\left(\frac{K_z^3}{3} + \zeta K_z\right) + i \int_0^\infty dK_z \sin\left(\frac{K_z^3}{3} + \zeta K_z\right), \end{aligned} \quad (3.3)$$

where  $\zeta$  is a real-valued parameter. Note that the other relevant integral is

$$\int_{-\infty}^0 dK_z \exp\left[i\frac{K_z^3}{3} + i\zeta K_z\right] = [I(\zeta)]^*. \quad (3.4)$$

Both the integrals involved in the real and imaginary parts of Eq. (3.3) can be solved in terms of Airy-related functions (Olver *et al.* 2010):

$$\int_0^\infty dK_z \cos\left(\frac{K_z^3}{3} + \zeta K_z\right) = \pi \text{Ai}(\zeta), \quad \int_0^\infty dK_z \sin\left(\frac{K_z^3}{3} + \zeta K_z\right) = \pi \text{Gi}(\zeta), \quad (3.5)$$

where  $\text{Ai}$  denotes the Airy function and  $\text{Gi}$  denotes the Scorer function. These functions are plotted in Fig. 1 for reference.

One therefore obtains

$$I(\zeta) = \pi [\text{Ai}(\zeta) + i \text{Gi}(\zeta)]. \quad (3.6)$$

This implies that the incoming and outgoing wavefields can be expressed as

$$\psi_{\text{in, out}}(\mathbf{X}) = \pi \int d\mathbf{K}_x \tilde{\psi}_0(\mathbf{K}_x) e^{i\mathbf{K}_x \cdot \mathbf{X}} [\text{Ai}(|\mathbf{K}_x|^2 - L) \pm i \text{Gi}(|\mathbf{K}_x|^2 - L)], \quad (3.7)$$

where the top (+) sign corresponds to the incoming wavefield and the bottom (−) sign corresponds to the outgoing wavefield. Again, we emphasize that these are exact relationships.

### 3.2. Fourier Inversion to obtain general solution

Let us now obtain the desired boundary-value solution (in coordinate space) using Eq. (3.7). To do so, let us perform an FT with respect to only the transverse coordinates  $\mathbf{X}$ . Analogous to Eq. (2.5), this transverse FT takes the form:

$$\widehat{\psi}_{\text{in}}(\mathbf{K}_x) = \int \frac{d\mathbf{X}}{(2\pi)^N} \psi_{\text{in}}(\mathbf{X}) e^{-i\mathbf{K}_x \cdot \mathbf{X}}, \quad (3.8a)$$

$$\psi_{\text{in}}(\mathbf{X}) = \int d\mathbf{K}_x \widehat{\psi}_{\text{in}}(\mathbf{K}_x) e^{i\mathbf{K}_x \cdot \mathbf{X}}. \quad (3.8b)$$

Then, we can clearly identify from Eq. (3.7) the relationship between the transverse FT and the standard FT images of  $\psi$ :

$$\widehat{\psi}_{\text{in}}(\mathbf{K}_x) = \pi \widetilde{\psi}_0(\mathbf{K}_x) [\text{Ai}(|\mathbf{K}_x|^2 - L) + i \text{Gi}(|\mathbf{K}_x|^2 - L)]. \quad (3.9)$$

Since the quantity  $\text{Ai}(|\mathbf{K}_x|^2 - L) + i \text{Gi}(|\mathbf{K}_x|^2 - L)$  is always nonzero (see Appendix A), we can then invert the relationship (3.9) to obtain

$$\widetilde{\psi}_0(\mathbf{K}_x) = \frac{1}{\pi} \frac{\widehat{\psi}_{\text{in}}(\mathbf{K}_x)}{\text{Ai}(|\mathbf{K}_x|^2 - L) + i \text{Gi}(|\mathbf{K}_x|^2 - L)}. \quad (3.10)$$

The general solution can then be written as

$$\psi(\mathbf{X}, Z) = \int d\mathbf{K}_x \frac{2 \text{Ai}(|\mathbf{K}_x|^2 + Z - L) \widehat{\psi}_{\text{in}}(\mathbf{K}_x)}{\text{Ai}(|\mathbf{K}_x|^2 - L) + i \text{Gi}(|\mathbf{K}_x|^2 - L)} e^{i\mathbf{K}_x \cdot \mathbf{X}}, \quad (3.11)$$

where  $\widehat{\psi}_{\text{in}}(\mathbf{K}_x)$  is the spectrum of the incoming beam, related to the prescribed boundary value via Eq. (3.8a). In essence, we have determined the arbitrary function  $\widetilde{\psi}_0(\mathbf{K}_x)$  in Eq. (2.8) that matches to a prescribed boundary condition  $\psi_{\text{in}}(\mathbf{X})$  *exactly*, without appealing to asymptotic approximations (Orlov and Tropkin 1980; Maj *et al.* 2009; Lopez *et al.* 2023) that necessarily restrict the validity of the resulting expressions.

As a sanity check, one can confirm that Eq. (3.11) reproduces the known result when  $\psi_{\text{in}}(\mathbf{X})$  is a constant; in this case,  $\widehat{\psi}_{\text{in}}(\mathbf{K}_x) \propto \delta(\mathbf{K}_x)$  such that subsequent integration gives  $\psi(\mathbf{X}, Z) \propto \text{Ai}(Z - L)$  as desired. Also, note that the incoming and outgoing components to Eq. (3.11) at  $Z = 0$  can be identified by performing the re-arrangement

$$\frac{2 \text{Ai}(|\mathbf{K}_x|^2 - L)}{\text{Ai}(|\mathbf{K}_x|^2 - L) + i \text{Gi}(|\mathbf{K}_x|^2 - L)} = 1 + \frac{\text{Ai}(|\mathbf{K}_x|^2 - L) - i \text{Gi}(|\mathbf{K}_x|^2 - L)}{\text{Ai}(|\mathbf{K}_x|^2 - L) + i \text{Gi}(|\mathbf{K}_x|^2 - L)}. \quad (3.12)$$

The incoming or outgoing component corresponds to the subsequent integration of the first or second factor, respectively. In particular, one recovers Eq. (3.8b) exactly.

## 4. Special case: Incident Gaussian beam in two dimensions

Let us now consider the case when the incoming wavefield is a Gaussian beam, which is of practical importance. We will also specialize to only consider 2-D propagation ( $N = 1$ ), since this will facilitate comparisons with other published formulas in the literature (Lopez *et al.* 2023; Orlov and Tropkin 1980; Maj *et al.* 2009). Specifically, we take

$$\psi_{\text{in}}(X) = E_0 \exp\left(i\sqrt{L} X \sin\theta - i\frac{X^2 \cos^2\theta}{2\sqrt{L} q_c}\right), \quad (4.1)$$

where  $E_0$  is a constant and  $q_c$  is the complex beam parameter normalized by the plasma

lengthscale  $\ell$ , with  $\text{Im}(q_c) \geq 0$ . Note that we have made use of the relationship

$$\frac{\omega \delta_a}{c} = \sqrt{L}. \quad (4.2)$$

Note also that one has

$$-\frac{i}{q_c} = -i \frac{\text{Re}(q_c)}{|q_c|^2} - \frac{\text{Im}(q_c)}{|q_c|^2}. \quad (4.3)$$

Hence, one can identify  $|q_c|^2/\text{Re}(q_c)$  as the radius of curvature and  $\sqrt{2L^{-3/2}|q_c|^2/\text{Im}(q_c)}$  as the beam waist (both normalized by  $\ell$ ). Focusing occurs when  $\text{Re}(q_c) > 0$ . The linear phase term in Eq. (4.1) simply rotates the phasefronts according to the angle of incidence  $\theta$  (with  $\theta = 0$  being normal incidence), while the additional factor of  $\cos^2 \theta$  in the quadratic phase term in Eq. (4.1) accounts for the stretching that occurs for oblique incidence. It is also worth mentioning that when  $\theta \neq 0$ , Eq. (4.1) corresponds to a well-collimated beam (long Rayleigh range) such that the variation of  $q_c$  along the incident boundary  $z = 0$  can be neglected (Belyaev *et al.* 2024).

#### 4.1. Exact solution

The transverse spectrum of the incoming wavefield is computed to be

$$\widehat{\psi}_{\text{in}}(K_x) = \mathcal{E} \exp \left[ \frac{i}{2} \sqrt{L} q_c \frac{(K_x - \sqrt{L} \sin \theta)^2}{\cos^2 \theta} \right], \quad (4.4)$$

where  $\mathcal{E} \doteq E_0 \sqrt{\frac{\sqrt{L} q_c}{2\pi i \cos^2 \theta}}$  is the overall constant. Equation (3.11) therefore takes the form

$$\begin{aligned} \psi(X, Z) = \mathcal{E} \int dK_x & \frac{2 \text{Ai}(K_x^2 + Z - L)}{\text{Ai}(K_x^2 - L) + i \text{Gi}(K_x^2 - L)} e^{iK_x X} \\ & \times \exp \left[ \frac{i}{2} \sqrt{L} q_c \frac{(K_x - \sqrt{L} \sin \theta)^2}{\cos^2 \theta} \right]. \end{aligned} \quad (4.5)$$

Equation (4.5) depends on four free parameters, three that characterize the boundary value of the incident beam and one that characterizes the medium. They are: (i)  $L$ , the medium lengthscale normalized by  $\delta_a$  defined in Eq. (2.2), related to normalization by the vacuum wavelength via Eq. (4.2); (ii)  $\text{Re}(q_c)$ , which parameterizes the incident radius of curvature normalized by the medium lengthscale; (iii)  $\text{Im}(q_c) \geq 0$ , which parameterizes the incident beam waist normalized by the medium lengthscale; and (iv)  $\theta \in [0, \pi/2)$ , the angle of incidence with respect to the direction of inhomogeneity  $Z$ .

#### 4.2. Oblique Injection as rigid translation and focal shift

Although the injection angle is nominally a free parameter, when the complex beam parameter is purely real,  $\text{Im}(q_c) = 0$ , then the injection angle  $\theta$  can also be removed by a coordinate transformation, up to an overall phase. Indeed, by completing the square, the initial condition (4.1) can be rewritten as:

$$\psi_{\text{in}}(X) = \mathcal{G} \left( X - L q_c \frac{\tan \theta}{\cos \theta}, L, \frac{q_c}{\cos^2 \theta} \right) \exp \left( \frac{i}{2} L^{3/2} q_c \tan^2 \theta \right) \quad (4.6)$$

where  $\mathcal{G}$  is the Gaussian profile of the incoming beam at normal incidence:

$$\mathcal{G}(X; L, q_c) = E_0 \exp \left( -i \frac{X^2}{2\sqrt{L} q_c} \right). \quad (4.7)$$

Clearly, when  $\text{Im}(q_c) = 0$ , Eq. (4.6) corresponds to rigid translation  $\Delta$  in the transverse  $X$  direction and a transformed focal length  $q_{c,\text{eff}}$  given by

$$\Delta = Lq_c \frac{\tan \theta}{\cos \theta}, \quad q_{c,\text{eff}} = \frac{q_c}{\cos^2 \theta}. \quad (4.8)$$

In particular, it was shown in Lopez *et al.* (2023) that critical focusing occurs at normal incidence when  $q_c = 2$ . Hence, for oblique incidence the critical focusing occurs when

$$q_{c,\text{crit}} = 2 \cos^2 \theta. \quad (4.9)$$

Note that these expressions (4.8) and (4.9) do not contain the additional Goos-Hanchen and focal shifts contained in the analogous formula from Lopez *et al.* (2023), since these phenomena are only present with a finite beam waist (McGuirk and Carniglia 1977). Hence, one should use these expressions rather than those of Lopez *et al.* (2023) when the beam waist is sufficiently large.

#### 4.3. Example: Softened critical focusing with finite beam waist

As discussed in Lopez (2023), the peak intensity of a critically focused wave [Eq. (4.9) being satisfied] can exceed the standard Airy intensity peak by orders of magnitude<sup>†</sup>. However, this only occurs when the beam waist is formally infinite. At normal incidence, the characteristic ‘detuning width’ to still achieve critical focusing is  $\Delta_q = 1/\sqrt{L}$  (Lopez *et al.* 2023); if this is entirely accounted for by a finite beam waist [ $\text{Im}(q_c) \neq 0$ ], then Eq. (4.8) implies that for critical focusing to occur, one must have

$$\text{Im}(q_c) \lesssim \frac{\cos^2 \theta}{\sqrt{L}}, \quad (4.10a)$$

or equivalently in terms of the beam waist  $W$  [defined following Eq. (4.3)]:

$$\frac{W}{\delta_a} \gtrsim \sqrt{L} \cos \theta. \quad (4.10b)$$

To obtain Eq. (4.10b), one must assume that  $q_{c,\text{crit}} \gg \text{Im}(q_c)$  given by Eq. (4.10a), which is equivalent to the condition that  $L \gg 1$ .

Figures 2 - 4 demonstrate how the hyperbolic umbilic diffraction pattern corresponding to critical focusing gets destroyed by a finite beam waist at various values of  $\theta$ , confirming the prediction of Eq. (4.10b). [Note that they also confirm the formulas (4.8) and (4.9) relating oblique injection with translations and focal shifts for infinitely wide beams.] Also shown are cases when the beam waist is minimized at fixed  $\text{Re}(q_c)$  [which occurs for  $\text{Im}(q_c) = \text{Re}(q_c)$ ], and when  $\text{Im}(q_c) \gg \text{Re}(q_c)$ . By softening the hyperbolic umbilic caustic, the peak intensity decreases with increasing  $\text{Im}(q_c)$ ; this has clear consequences for applications the desire strong focusing near the turning point (such as those discussed in the introduction) and suggests that one should minimize  $\text{Im}(q_c)$  as much as possible.

<sup>†</sup> The ratio of the two intensities formally diverges in the short-wavelength asymptotic limit.

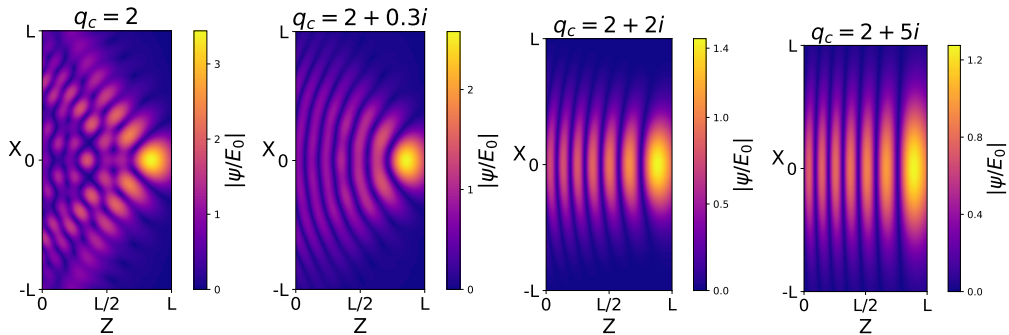


**Figure 2:** Morphology of the hyperbolic umbilic caustic that occurs at critical focusing (4.9) as  $\text{Im}(q_c)$  is increased from zero at normal incidence ( $\theta = 0$ ) with  $L = 10$ . The plots are obtained from numerically integrating the exact solution (4.5). From left to right, the figures show the diffraction pattern at critical focusing, at the expected detuning value of  $\text{Im}(q_c)$  (4.10a), at the  $\text{Im}(q_c)$  that minimizes the beam waist, and at  $\text{Im}(q_c) \gg \text{Re}(q_c)$ . Note that the colorbar axis changes for each plot.

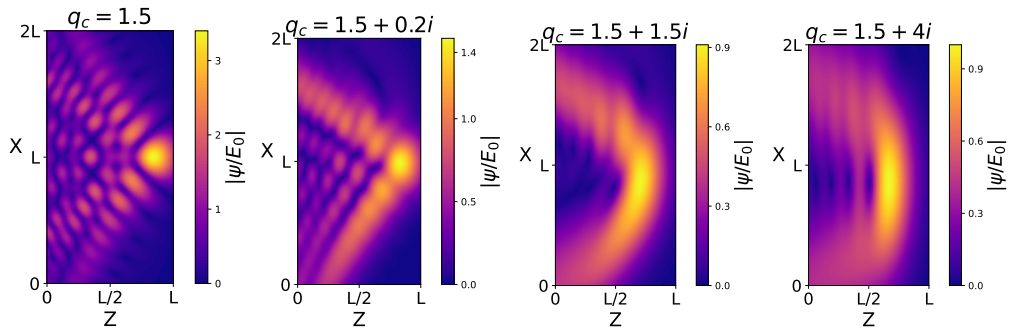


**Figure 3:** Same as Fig. 2 but for  $\theta = 30^\circ$ .

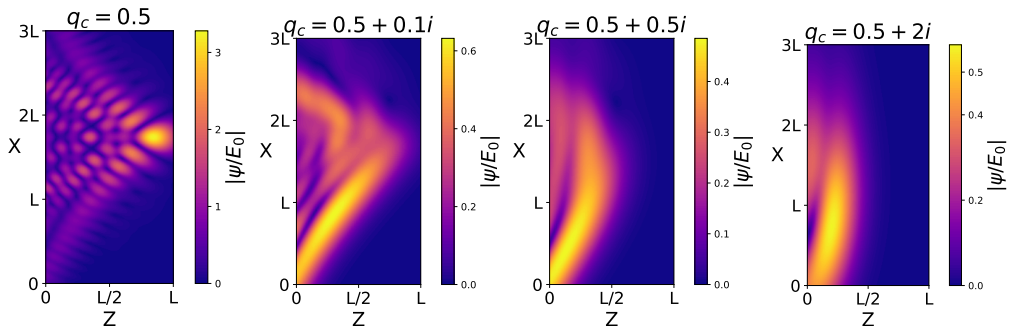


**Figure 4:** Same as Fig. 2 but for  $\theta = 60^\circ$ .

#### 4.4. Comparison with existing asymptotic formulas

For comparison purposes, let us also list the existing asymptotic formulas provided by Orlov and Tropkin (1980), Maj *et al.* (2009), and Lopez *et al.* (2023), which we shall refer to respectively as the O80, the M09, and the L23 formulas. (We reiterate that to the best of our knowledge, only asymptotic solutions to the linear layer problem with prescribed boundary value have appeared in the literature.) These formulas are given for



the initial condition (4.1) as<sup>†</sup>

$$\begin{aligned} \psi_{\text{O80}}(X, Z) = & \mathcal{E} \int dK_x \frac{2 \text{Ai}(K_x^2 + Z - L)}{\text{Ai}(K_x^2 - L) - i \text{Ai}'(K_x^2 - L) / \sqrt{L - K_x^2}} e^{iK_x X} \\ & \times \exp \left[ \frac{i}{2} \sqrt{L} q_c \frac{(K_x - \sqrt{L} \sin \theta)^2}{\cos^2 \theta} \right], \end{aligned} \quad (4.11)$$

$$\begin{aligned} \psi_{\text{M09}}(X, Z) = & \mathcal{E} \frac{2\pi}{\sqrt{\pi i}} \int_{-\sqrt{L}}^{\sqrt{L}} dK_x (L - K_x^2)^{1/4} \text{Ai}(K_x^2 + Z - L) e^{iK_x X} \\ & \times \exp \left[ \frac{i}{2} \sqrt{L} q_c \frac{(K_x - \sqrt{L} \sin \theta)^2}{\cos^2 \theta} + i \frac{2}{3} (L - K_x^2)^{3/2} \right], \end{aligned} \quad (4.12)$$

$$\begin{aligned} \psi_{\text{L23}}(X, Z) = & \mathcal{E}_L \int dK_x \text{Ai}(K_x^2 + Z - L) e^{iK_x X} \\ & \times \exp \left[ \frac{i}{2} \sqrt{L} \frac{q_c - 2 \cos 2\theta \cos \theta}{\cos^2 \theta} \left( K_x - \sqrt{L} \sin \theta \frac{q_c + \sin 2\theta \sin \theta}{q_c - 2 \cos 2\theta \cos \theta} \right)^2 \right], \end{aligned} \quad (4.13)$$

where we have introduced

$$\mathcal{E}_L = \mathcal{E} 2\pi \sqrt{\frac{\sqrt{L} \cos \theta}{\pi i}} \exp \left( \frac{i}{6} L^{3/2} \cos^3 \theta \frac{4q_c - 7 \cos \theta - \cos 3\theta}{q_c - \cos \theta - \cos 3\theta} \right). \quad (4.14)$$

As discussed in Appendix B, each of the formulas (4.11) - (4.13) are asymptotically equivalent to the exact solution (4.5) when  $L$  is much greater than all wavevectors contained within the incoming spectrum. The region of validity for this condition is plotted in Fig. 5. That said, for finite  $L - K_x^2$ , each of the listed formulas have some shortcomings: Eq. (4.11) contains a singularity at  $L = K_x^2$  that is clearly unphysical; Eq. (4.12) truncates the integral for  $K_x^2 \geq L$  and thereby neglects evanescent contributions to the total field; and Eq. (4.13) performs a subsidiary Taylor expansion in  $K_x^2$  to highlight the caustic structure, with additional loss of accuracy expected as a result. This includes the incorrect predictions for the transverse shift  $\Delta$  and the focal shift for a wide beam at oblique incidence discussed in the previous section.

## 5. Special case: Speckled plane wave at normal incidence

Let us now consider an incoming field obtained via paraxial propagation from a lens aperture with focal length  $d$  in 2-D. If the field is evaluated at best focus (i.e., following a propagation distance  $d$ ), then the (far-field) Fraunhofer diffraction formula gives the solution to be<sup>‡</sup>

$$\psi_{\text{in}}(X) = E_0 \int dY \psi_0(Y) \exp \left( -i \frac{\sqrt{L}}{D} XY \right), \quad (5.1)$$

where  $D = d/\delta_a$  and  $\psi_0$  is the field profile that illuminates the lens aperture. Let us choose  $\psi_0$  to be a uniformly illuminated RPP array that consists of  $M$  identical elements

<sup>†</sup> Note that we have corrected an error in Maj *et al.* (2009); their Eq. (17) is missing an extra factor of  $\omega \ell / c$  in the exponent.

<sup>‡</sup> See, for example, the general discussion in Lopez (2022), and specifically the cascaded system given by the matrix product of their Eq. 3.137 and Eq. 3.146.

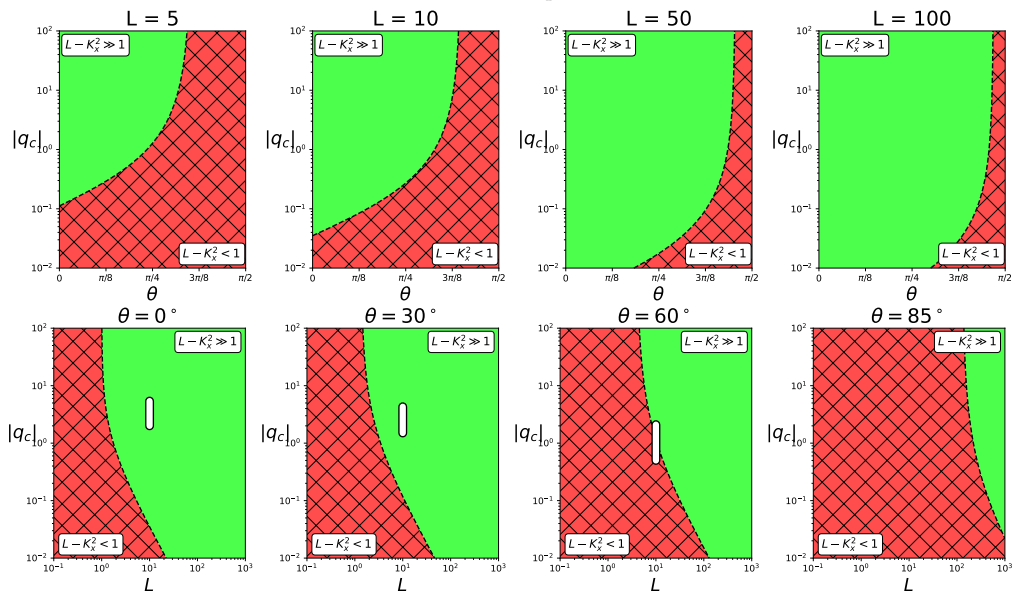


**Figure 5:** Validity boundary for the asymptotic solutions (4.11) - (4.13) as determined by Eq. (B 1), either as a function of  $q_c$  and  $\theta$  for specified  $L$  (top row) or as a function of  $q_c$  and  $L$  for specified  $\theta$  (bottom row). Within the red hatched region, only the exact solution (4.5) remains valid. No valid asymptotic region exists for  $L \leq 1$  and for  $\theta = \pi/2$ . The white vertical rectangle in the figures for  $\theta = 0^\circ$ ,  $\theta = 30^\circ$ , and  $\theta = 60^\circ$  corresponds to the range of special cases considered in Figs. 2, 3, and 4 respectively.

of width  $W/M$  (so the total width is  $W$ , normalized by  $\delta_a$  as usual):

$$\psi_0(Y) = \sum_{m=-\frac{M-1}{2}}^{\frac{M-1}{2}} e^{i\phi_m} \text{rect}\left(\frac{M}{W}Y - m\right), \quad (5.2)$$

where  $\phi_m$  is the corresponding phase shift, set to be either 0 or  $\pi$  (Dixit *et al.* 1993). We take  $M$  to be odd for simplicity. Also,  $\text{rect}(x)$  is the unit rectangular function that is nonzero only within the interval  $-1/2 \leq x \leq 1/2$ . One then has

$$\hat{\psi}_{\text{in}}(K_x) = E_0 \frac{D}{\sqrt{L}} \sum_{m=1}^M e^{i\phi_m} \text{rect}\left(\frac{M}{\eta}K_x + m\right), \quad (5.3)$$

where we have introduced the coupling coefficient  $\eta$  as

$$\eta = \frac{\sqrt{L}}{f_{\#}}, \quad f_{\#} \doteq \frac{D}{W}. \quad (5.4)$$

Note that  $f_{\#}$  is the f-number of the launching aperture. Consequently, Eq. (3.11) reads

$$\begin{aligned} \psi(X, Z) &= E_0 \frac{D}{\sqrt{L}} \sum_{m=1}^M \exp\left(i\phi_m + i\eta X \frac{m}{M}\right) \\ &\times \int_{-\frac{\eta}{2M}}^{\frac{\eta}{2M}} dK_x \frac{2 \text{Ai}[(K_x + \eta \frac{m}{M})^2 + Z - L]}{\text{Ai}[(K_x + \eta \frac{m}{M})^2 - L] + i \text{Gi}[(K_x + \eta \frac{m}{M})^2 - L]} e^{iK_x X}. \end{aligned} \quad (5.5)$$

Equation (5.5) is the exact solution for the incoming speckled wavefield given in

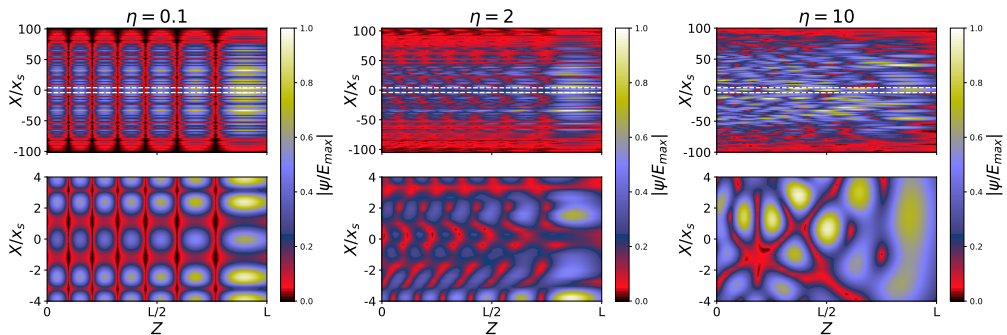


**Figure 6:** Exact solution (5.5) for an incoming speckled wavefield at various values of the coupling coefficient  $\eta$  and  $L = 10$  and  $M = 100$  RPP elements. The transverse direction is normalized by the nominal speckle width (Michel 2023), which in the normalized coordinates is given by  $x_s \sim 2\pi/\eta$ . For each set of figures, the top figure shows the beam profile over the nominal envelope width  $Mx_s$ , while the bottom figure shows the region within the dashed lines of the top figure.

Eq. (5.1). A complete statistical study of this solution is beyond the scope of the present paper, but one property can be seen immediately. Let us take the number of RPP elements to be sufficiently large,  $M \gg \eta$ , such that the integral in (5.5) can be approximated by its central value. This yields

$$\psi(X, Z) \approx E_0 \frac{D}{\sqrt{L}} \sum_{m=1}^M \exp\left(i\phi_m + i\eta X \frac{m}{M}\right) \frac{2 \text{Ai}\left[\left(\eta \frac{m}{M}\right)^2 + Z - L\right]}{\text{Ai}\left[\left(\eta \frac{m}{M}\right)^2 - L\right] + i \text{Gi}\left[\left(\eta \frac{m}{M}\right)^2 - L\right]}. \quad (5.6)$$

Hence when the coupling is small,

$$\eta \ll 1, \quad (5.7)$$

the transverse speckle pattern and the longitudinal Airy pattern are decoupled from each other. In this limit one needs to simply multiply a given incoming speckle pattern with a single Airy profile along  $Z$  to obtain the full solution.

As shown by the definition of  $\eta$  in Eq. (5.4), decoupling occurs when a large f-number beam is launched into a plasma with relatively short lengthscale. Conversely, a small f-number beam launched into a plasma with shallow gradient will exhibit a significantly more complicated longitudinal profile. This is demonstrated in Fig. 6 and Fig. 7, which compare the solution (5.5) for a larger and smaller coupling coefficient. The decoupled speckles exhibit a regular periodicity along the propagation direction, while the coupled speckles exhibit a considerably more complicated interference pattern. The longitudinal swelling of the coupled speckles also differs significantly from the standard Airy swelling, with the maximum intensity no longer necessarily occurring near the turning point.

## 6. Conclusion

In this work, the classic problem of an electromagnetic wave propagating in a linearly varying index of refraction (the ‘linear-layer problem’) is revisited. Specifically, we consider what the wavefield throughout the domain is given a prescribed incoming field at the boundary transverse to the direction of inhomogeneity. Previous studies have only obtained asymptotic solutions to this problem setup; here we obtain the exact result by using a spectral matching scheme. The resulting solution (3.11) is expressed as an integral involving the Fourier transform of the prescribed incoming boundary field multiplied by a kernel involving the familiar Airy function and also the related Scorer function. The

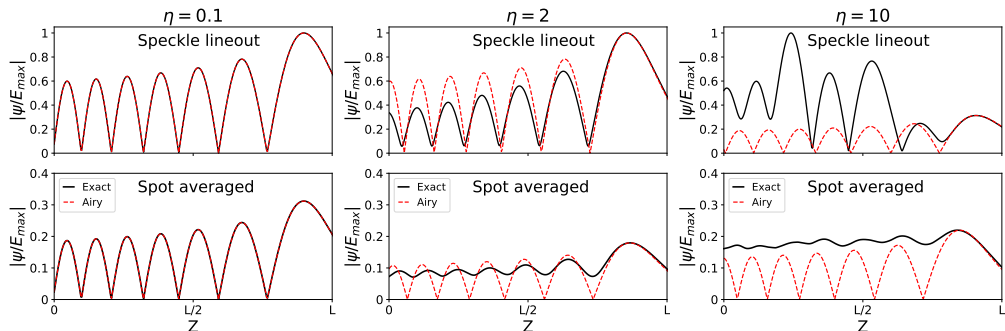


**Figure 7:** Lineouts along  $Z$  (top) of the exact solution presented in Fig. 6 at the location of the brightest speckle, along with the solution averaged over the entire  $X$  range (bottom). Also shown are Airy function fits obtained by matching the first peak value and location for each respective plot.

kernel is never singular and therefore is uniformly valid regardless the relative sizes of the launched wavelength and the medium lengthscale.

An incident Gaussian beam is then studied as a test case, with corresponding exact solution given by Eq. (4.5). It is shown that when the beam is sufficiently wide (i.e., a Gaussian-focused plane wave), oblique angle of incidence results in a simple shift of the focal length and a rigid translation of the diffraction pattern. Explicit expressions are provided by Eqs. (4.8) and (4.9), which modify the analogous expressions presented in Lopez *et al.* (2023) by removing the Goos–Hanchen shifts that cannot arise without a finite beam waist. That said, the general prediction of Lopez *et al.* (2023) that the hyperbolic umbilic caustic is structurally stable with respect to angle of incidence still holds true.

It is then demonstrated how the hyperbolic umbilic caustic corresponding to critical focusing of a wide beam gets softened and ultimately disappears as the beam waist is reduced. This softening of the caustic is accompanied by a reduction in the peak intensity obtained by the Gaussian beam at the turning point, which suggests that for applications reliant on the intensity of a wavefield near a turning point, one should make the imaginary part of the complex beam parameter for the launched beam as small as possible. More quantitatively, the hyperbolic umbilic caustic deteriorates once the beam waist  $W$  becomes smaller than  $W/\delta_a \lesssim \sqrt{L}$ , where  $\delta_a$  is the Airy skin depth (2.2) and  $L$  is the medium lengthscale normalized by  $\delta_a$ . This means that beam-tracing solutions (Maj *et al.* 2009, 2010) are fundamentally incapable of describing the hyperbolic umbilic caustic, since the validity of beam-tracing requires  $W/\delta_a \sim \sqrt[4]{L}$  (with  $L$  also being large). Advanced ray-tracing methods (Lopez and Dodin 2020, 2021, 2022; Lopez *et al.* 2024; Højlund *et al.* 2024) may be able to describe it, however, as they have no such restriction on the beam waist. Conversely, this analysis suggests that any anomalous focusing observed in beam-tracing solutions is not due to the hyperbolic umbilic caustic, but instead due to the relatively simpler Airy (fold) caustic.

Finally, an incident speckled wavefield is also studied. It had been observed previously in numerical parameter scans that large  $f$ -number beams in steep gradients experience decoupled speckle and Airy behavior (Lopez *et al.* 2021), but no concise coupling parameter had been identified. Here we derive the coupling parameter to be  $\eta = \sqrt{L}/f_{\#}$ , and show that speckles only influence the longitudinal profile of the total wavefield when  $\eta \gtrsim 1$ , or equivalently, when  $\ell \gtrsim \lambda f_{\#}^3/2\pi$ . This suggests that a reduced model of laser beams near turning points is obtained in the low-coupling regime by simply

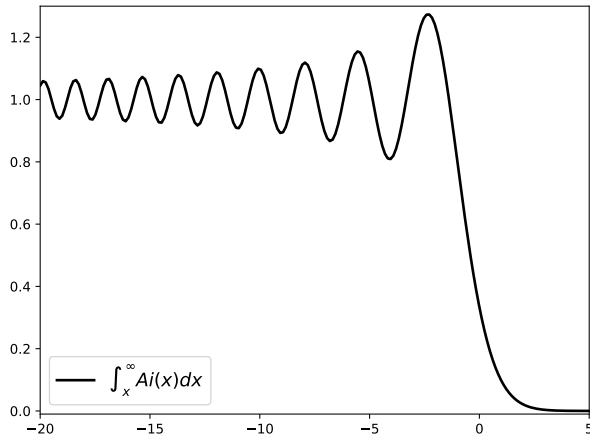


**Figure 8:** Evaluating the integral  $\int_x^\infty \text{Ai}(z)dz$  for different values of the lower limit  $x$ . Note that since  $\text{Ai}(\zeta) > 0$  for  $\zeta > 0$ , the integral is manifestly positive for  $x > 0$  and asymptotes to zero as  $x \rightarrow +\infty$ .

multiplying the transverse speckle pattern with the Airy swelling factor. In the strong-coupling regime, however, the interference patterns are seen to be considerably more complicated, and more work remains to develop reduced models in this limit. To put this finding in context, in terms of the NIF laser (Spaeth *et al.* 2016) the transition to strong coupling occurs for a 351 nm f/22 beam when the plasma lengthscale exceeds 3.7 mm, or when it exceeds 0.2 mm for an f/8 quad beam.

## Acknowledgements

The author thanks Dr. Juan Ruiz Ruiz of Oxford University for useful conversations. This work is partly supported by STFC (grant number ST/W000903/1).

## Appendix A. Interlacing of Airy and Scorer zeros

It is important to note

$$\text{Ai}(x) \pm i \text{Gi}(x) \neq 0 \quad (\text{A } 1)$$

because the zeros of Ai and Gi never overlap. Since this fact of Gi is difficult to find in the literature<sup>†</sup>, we shall present a simple proof here for completeness.

By definition, one has (Olver *et al.* 2010)

$$\text{Gi}(x) = \text{Bi}(x) \int_x^\infty \text{Ai}(z)dz + \text{Ai}(x) \int_0^x \text{Bi}(z)dz. \quad (\text{A } 2)$$

If one evaluates Gi at a zero of Ai, denoted  $x_0$  (and one notes that  $x_0 < 0$ ), one obtains

$$\text{Gi}(x_0) = \text{Bi}(x_0) \int_{x_0}^\infty \text{Ai}(z)dz. \quad (\text{A } 3)$$

Since the zeros of Ai and Bi are interlaced, one has  $\text{Bi}(x_0) \neq 0$ . Also, numerical

<sup>†</sup> For example, Gil *et al.* (2003) only compares the zeros of Gi and Bi, not Gi and Ai as we require here.

investigation (Fig. 8) shows that

$$\int_x^\infty \text{Ai}(z) dz > 0 \quad (\text{A4})$$

for all values of  $x$ . Hence  $\text{Gi}(x_0) \neq 0$ . QED.

## Appendix B. Asymptotic equivalence of the exact solution with other published expressions

Here we show that the exact solution (4.5) is asymptotically equivalent to the other expressions listed in Eqs. (4.11) - (4.13) in the large  $L \rightarrow \infty$  limit. Specifically, we take  $L$  to be much larger than all  $K_x^2$  that appear in the incoming spectrum, requiring

$$L \left[ 1 - \left( \sin \theta + \frac{\cos \theta}{L^{3/4} \sqrt{|q_c|}} \right)^2 \right] \gg 1. \quad (\text{B1})$$

Note that to derive Eq. (B1), we have estimated the mean wavevector to be  $\sqrt{L} \sin \theta$  and the spectral width to be  $\cos \theta / |q_c|^{1/2} L^{1/4}$ , per Eq. (4.4). When Eq. (B1) is satisfied, we can take  $\zeta \doteq L - K_x^2$  to be sufficiently large, viz.  $\zeta \gg 1$ , such that the following asymptotic approximations hold:

$$\text{Ai}(-\zeta) \sim \frac{\cos\left(\frac{2}{3}\zeta^{3/2} - \frac{\pi}{4}\right)}{\sqrt{\pi}\zeta^{1/4}}, \quad (\text{B2a})$$

$$\text{Ai}'(-\zeta) \sim \zeta^{1/4} \frac{\sin\left(\frac{2}{3}\zeta^{3/2} - \frac{\pi}{4}\right)}{\sqrt{\pi}}, \quad (\text{B2b})$$

$$\text{Gi}(-\zeta) \sim -\frac{\sin\left(\frac{2}{3}\zeta^{3/2} - \frac{\pi}{4}\right)}{\sqrt{\pi}\zeta^{1/4}}. \quad (\text{B2c})$$

### B.1. Asymptotic equivalence with O80 formula

The exact solution (4.5) and the O80 formula (4.11) differ only via the denominator in the integrand; Eq. (4.5) has  $\text{Ai}(-\zeta) + i \text{Gi}(-\zeta)$  while Eq. (4.11) has  $\text{Ai}(-\zeta) - i \text{Ai}'(-\zeta) / \sqrt{\zeta}$ . When  $\zeta \gg 1$ , the asymptotic relations (B2) then give

$$\text{Ai}(-\zeta) + i \text{Gi}(-\zeta) \sim \frac{\exp\left(-i\frac{2}{3}\zeta^{3/2} + i\frac{\pi}{4}\right)}{\sqrt{\pi}\zeta^{1/4}}, \quad (\text{B3a})$$

$$\text{Ai}(-\zeta) - i \frac{\text{Ai}'(-\zeta)}{\sqrt{\zeta}} \sim \frac{\exp\left(-i\frac{2}{3}\zeta^{3/2} + i\frac{\pi}{4}\right)}{\sqrt{\pi}\zeta^{1/4}}. \quad (\text{B3b})$$

The integrands to both formulas have the same asymptotic limit when  $\zeta \gg 1$ ; hence the two formulas should agree when Eq. (B1) is satisfied. That said, it is clear that the integrand of Eq. (4.11) has a singularity at  $\zeta = 0$ , so it will not hold uniformly in  $\zeta$ .

### B.2. Asymptotic equivalence with M09 formula

Let us again assume that  $\zeta \gg 1$ . Applying the asymptotic formula (B3a) to Eq. (4.5) then gives the integrand of Eq. (4.12). However, Eq. (4.12) also restricts the integration bounds from the entire real line to the interval  $K_x \in [-\sqrt{L}, \sqrt{L}]$ . This ensures that  $\zeta$  remains positive over the integration, but neglects evanescent modes (with long decay lengths) that may contribute to the exact solution. These modes should be absent when Eq. (B1) is well-satisfied, but may be present when it is only marginally true.

## B.3. Asymptotic equivalence with L23 formula

Again, let us take  $\zeta \gg 1$  and apply (B3a) to Eq. (4.5) to obtain the integrand of Eq. (4.12). We then perform a subsidiary expansion in the limit of small spectral width  $\Delta_k \doteq K_x - K_0$  about the mean wavevector  $K_0 = \sqrt{L} \sin \theta$ . This condition reads  $L \cos^2 \theta \gg |(\Delta_k + 2K_0)\Delta_k|$ , which is equivalent to Eq. (B1) when the same estimate for  $\Delta_k$  is used. The lowest-order approximation for the amplitude gives

$$\zeta^{1/4} = L^{1/4} \sqrt{\cos \theta} + O(\Delta_k), \quad (\text{B4})$$

while a higher-order approximation for the phase gives

$$\frac{2}{3} \zeta^{3/2} = \frac{2}{3} L^{3/2} \cos^3 \theta - \epsilon L \sin 2\theta - \epsilon^2 \sqrt{L} \frac{\cos 2\theta}{\cos \theta} + O(\Delta_k^3). \quad (\text{B5})$$

Following some algebra, it can then be shown that inserting Eq. (B4) and (B5) into Eq. (4.5) recovers Eq. (4.13). Therefore, Eqs. (4.5) and (4.13) are asymptotically equivalent when Eq. (B1) is well-satisfied. epeq:LopezBEAM are asymptotically equivalent when Eq. (B1) is well-satisfied.

## REFERENCES

- V. L. Ginzburg, *Propagation of electromagnetic waves in plasma* (New York: Gordon and Breach, 1961).
- M. Ono, N. Bertelli, V. Shevchenko, H. Idei, and K. Hanada, *Phys. Rev. E* **106**, L023201 (2022a).
- M. Ono, N. Bertelli, and V. Shevchenko, *Nucl. Fusion* **62**, 106035 (2022b).
- V. H. Hall-Chen, F. I. Parra, and J. C. Hillesheim, *Plasma Phys. Control. Fusion* **64**, 095002 (2022).
- Y. I. Orlov and S. K. Tropkin, *Radiophys. Quantum Electron.* **23**, 979 (1980).
- O. Maj, G. V. Pereverzev, and E. Poli, *Phys. Plasmas* **16**, 062105 (2009).
- O. Maj, A. A. Balakin, and E. Poli, *Plasma Phys. Control. Fusion* **52**, 085006 (2010).
- N. A. Lopez, E. Kur, and D. J. Strozzi, *Phys. Rev. E* **107**, 055204 (2023).
- P. Michel, *Introduction to Laser-Plasma Interactions* (Cham: Springer, 2023).
- F. W. J. Olver, D. W. Lozier, R. F. Boisvert, and C. W. Clark, *NIST Handbook of Mathematical Functions* (Cambridge: Cambridge University Press, 2010).
- M. A. Belyaev, J. Banks, and T. Chapman, *Phys. Plasmas* **31**, 053901 (2024).
- M. McGuirk and C. K. Carniglia, *J. Opt. Soc. Am.* **67**, 103 (1977).
- N. A. Lopez, in *49th EPS Conference on Plasma Physics, EPS 2023* (arXiv:2309.15108, 2023) p. P2.011.
- N. A. Lopez, *Metaplectic geometrical optics*, *Ph.D. thesis*, Princeton University (2022).
- S. N. Dixit, I. M. Thomas, B. W. Woods, A. J. Morgan, M. A. Hessian, P. J. Wegner, and H. T. Powell, *Appl. Opt.* **32**, 2543 (1993).
- N. A. Lopez and I. Y. Dodin, *New J. Phys.* **22**, 083078 (2020).
- N. A. Lopez and I. Y. Dodin, *J. Opt.* **23**, 025601 (2021).
- N. A. Lopez and I. Y. Dodin, *Phys. Plasmas* **29**, 052111 (2022).
- N. A. Lopez, R. Højlund, and M. G. Senstius, arXiv:2406.01270 (2024).
- R. Højlund, M. G. Senstius, and S. K. Nielsen, arXiv:2402.03882 (2024).
- N. A. Lopez, E. Kur, T. D. Chapman, D. J. Strozzi, and P. A. Michel, *Bull. Am. Phys. Soc.* **66**, Abstract NP11.00063 (2021).
- M. L. Spaeth, K. R. Manes, D. G. Kalantar, P. E. Miller, J. E. Heebner, E. S. Bliss, D. R. Spec, T. G. Parham, P. K. Whitman, P. J. Wegner, P. A. Baisden, J. A. Menapace, M. W. Bowers, S. J. Cohen, T. I. Suratwala, J. M. Di Nicola, M. A. Newton, J. J. Adams, J. B. Trenholme, R. G. Finucane, R. E. Bonanno, D. C. Rardin, P. A. Arnold, S. N. Dixit, G. V. Erbert, A. C. Erlandson, J. E. Fair, E. Feigenbaum, W. H. Gourdin, R. A. Hawley, J. Honig, R. K. House, K. S. Jancaitis, K. N. LaFortune, D. W. Larson, B. J. Le Galloudec, J. D. Lindl, B. J. MacGowan, C. D. Marshall, K. P. McCandless, R. W.

- McCracken, R. C. Montesanti, E. I. Moses, M. C. Nostrand, J. A. Pryatel, V. S. Roberts, S. B. Rodrigues, A. W. Rowe, R. A. Sacks, J. T. Salmon, M. J. Shaw, S. Sommer, C. J. Stolz, G. L. Tietbohl, C. C. Widmayer, and R. Zacharias, *Fusion Sci. Technol.* **69**, 25 (2016).
- A. Gil, J. Segura, and N. M. Temme, *J. Approx. Theory* **120**, 253 (2003)